Available online at www.sciencedirect.com
ScienceDirect
Ceramics International 37 (2011) 2185–2191
CERAMICS INTERNATIONAL
www.elsevier.com/locate/ceramint

Direct observation of domain switching and crack nucleation in a piezoelectric material

C. Leach *, N.K. Ali, D.A. Hall

School of Materials, University of Manchester, Manchester M13 9PL, UK

Received 12 January 2011; received in revised form 2 March 2011; accepted 3 March 2011
Available online 9 March 2011

Abstract

The effect of an electric field on domain switching and fatigue induced crack nucleation and growth in a piezoelectric material of nominal composition $Pb(Zr_{0.5}, Ti_{0.5})O_3$ has been investigated. The ceramic was subjected to localised static and cyclic electric fields, which were applied via pairs of closely spaced surface-mounted electrodes, while simultaneously imaging the microstructure in the SEM. Electric field–polarisation hysteresis loops were also collected from the local region using the same electrodes.

Domain wall mobility was observed above a threshold electric field strength, as was microcracking. Cracks were seen to nucleate at grain boundaries, and were sometimes associated with microstructural features, such as pores. Crack propagation was mainly intergranular, and occurred preferentially in a direction parallel to the local field direction. Transgranular fracture was also observed, with the crack path being influenced by interaction with domain boundaries. Factors affecting domain switching and crack propagation are discussed in the context of the locally applied electric field.

Keywords: C. Mechanical properties; C. Piezoelectric properties; D. PZT; Domains

1. Introduction

Bulk lead zirconate titanate (PZT) piezoceramics are widely exploited in various applications including: sensors, actuators, transducers, transformers and filters [1,2]. In operation, many of these devices are subjected to large electric fields that give rise to significant local mechanical stresses, resulting in fatigue and degradation of electromechanical properties [3–6]. In order to understand the underlying mechanisms controlling these processes, several workers have studied the fine-scale mechanisms of failure in piezoelectric materials under electrical and mechanical loading. Many researches have suggested that electrical and mechanical fatigue of piezoelectric ceramics is predominantly due to the effects of domain switching during electric field cycling [7–13]. Electrical fatigue, associated with a reduction in switched charge and induced strain [14], has been attributed to a range of microstructural and microchemical features including: grain size, pore distribution, and chemical segregation effects [15]. Under cyclic voltage loading, mechanical degradation by crack nucleation and growth mechanisms has also been reported to occur [4,15,16]. At low electric fields (E), below the coercive field (E_C), crack propagation is attributed to the effect of domain switching due to stresses arising from the localisation of the electric field around crack tips [15,17]. Above E_C, crack propagation is believed to be due to localised stresses arising from differences in electric field strength between the cracked and uncracked regions [15]. A study of through-thickness cracks in bulk PZT established a threshold value of E, corresponding to $0.797E_C$, below which crack growth did not occur, but above which the propagation rate increased steadily, allowing a phenomenological model for the relationship between field strength and rate of crack growth to be developed [18].

Crack-growth experiments have been carried out on barium titanate (BT) [8,19], lead magnesium niobate–lead niobate (PMN–PT) solid solutions [20,21] and PZT [18,22] using pre-cracked bulk specimens and cyclic electric fields. A general preference for crack propagation perpendicular to the electric field direction was observed in unconstrained samples. A TEM-based study of single crystal PZT found that microcrack

* Corresponding author at: School of Materials, University of Manchester, Materials Science Building, Manchester M13 9PL, UK. Tel.: +44 161 306 3561.
E-mail address: colin.leach@manchester.ac.uk (C. Leach).

0272-8842/$36.00
doi:10.1016/j.ceramint.2011.03.012

nucleation occurred under both static and cyclic electric fields and noted an interaction between the preferred crack path and domain wall alignment [23].

In this study, SEM based local property measurement techniques have been used to measure electric field–polarisation hysteresis loops of localised regions within a PZT ceramic, on the 20 μm scale, using surface mounted electrodes, while making simultaneous in situ observation and characterisation of microstructural changes at the sample surface, including domain wall movements due to switching, and crack nucleation and growth under conditions of constant electric field and cyclic fatigue loading.

2. Experimental

$(Pb_{0.965}La_{0.01}Sr_{0.02})(Zr_{0.5}Ti_{0.5})O_3$ powder was prepared by a standard mixed oxide route using GPR grade starting powders. The sample composition was chosen to lie within the tetragonal phase region of the PZT phase diagram, close to the morphotropic phase boundary (MPB). Green compacts were uniaxially pressed at 400 MPa, and sintered in oxygen at 1225 °C for 2 h within a closed alumina crucible, which was covered with $PbZrO_3$ powder to limit lead loss. A cross-section of the sintered specimen was cut, ground flat and polished with diamond paste, followed by lapping with a colloidal silica suspension to give a strain-free surface suitable for imaging and electron backscattered pattern (EBSP) analysis. An array of 80 μm square Pt electrodes, with 20 μm separation, was sputtered onto the polished surface through a photolithographically applied lift-off mask. The sample was mounted in a Phillips XL30 FEGSEM, and observed using backscattered electron (BS) imaging under low energy beam conditions (8 kV, 1.5 nA) to prevent beam-induced specimen damage. Grain size was calculated using SEM images and a standard linear intercept method, applying a geometrical factor of 1.56 [24]. The orientation of twin planes and selected grain boundaries was determined by EBSP analysis using a HKL EBSP system mounted on the same SEM. Because of the low *c*/*a* ratio and the resolution limitations of EBSP indexing, crystal directions were calculated according to a cubic unit cell. Electrical contact to the surface electrodes was made using micromanipulator controlled tungsten probes and a custom-built voltage source was used to generate an electric field within the sample between pairs of adjacent electrodes. DC fields were allowed to stabilise for 60 s prior to imaging, and images were collected with the electric field 'on'. AC voltage cycling was carried out at 20 Hz. Each series of cycles was terminated with an identical poling pulse to ensure that images were collected under identical conditions to allow consistency of observation. Spatially localised polarisation–electric field hysteresis loops were collected via the same electrodes using proprietary software.

3. Results and discussion

3.1. Microstructure

The density of the ceramic was measured using the Archimedes method and found to be 98% of theoretical. There is some fine residual porosity, principally at triple points but also occasionally extending along grain boundaries. The grains are equiaxed, with a mean size of 6 ± 2 μm. Twinning is readily observed within the grains, although subsequent images contain significant noise due to the low-energy imaging conditions that were adopted in order to prevent beam-induced sample damage.

3.2. Static field behaviour

Fig. 1(a) shows a BS image of a PZT grain, located between a pair of electrodes situated 20 μm apart and located to the left and the right of the viewed area. The edge of the right-hand electrode is visible at the side of the image. Microstructural changes occurred throughout the material due to the application of an external electric field: we will use the example of this grain to illustrate in detail the typical behaviour. The twin plane orientations within this grain were indexed using a combination of EBSP and trace analysis, and are indicated in the figure, being a mixture of {1 1 0} and {1 0 0} types. A localised electric field was generated in the sample by applying a voltage across the electrodes. The magnitude and polarity of the applied electric field is defined here by the potential of the right-hand electrode (the edge of which is visible in the image) relative to the left-hand electrode, with the resultant electric field being oriented horizontally across the image. For voltages in the range 0 V to −130 V, the microstructure appeared to remain unchanged. However, when the voltage was increased to −135 V there was significant domain wall movement, bringing the twin configuration shown in Fig. 1(b) into contrast. The twin planes within this grain are now all of the {1 1 0} type and are aligned approximately perpendicular to the electric field direction. The associated strain has also resulted in the nucleation and propagation of an intergranular crack in a direction parallel to the electric field. This new twin arrangement was retained after the electric field was removed, although the crack was observed to close slightly, indicating some strain relaxation.

The electric field direction was then reversed by applying +135 V to the right-hand electrode. This led to further domain wall movement, and the formation of the twin microstructure shown in Fig. 1(c). The twin planes in contrast are now a mixture of {1 1 0} and {1 0 0} types, and generally lie at about 45° to the electric field direction. The intergranular crack has propagated further and forked along two grain boundaries, both of which lie at about 45° to the electric field direction. On removing the electric field, the twin microstructure immediately relaxed to that shown in Fig. 1(d). The fine twins that are now in contrast lie predominantly on {1 1 0} planes. There is also a prominent {1 1 1} twin running through the centre of the grain. It was possible to switch repeatedly between the twinning patterns shown in Fig. 1(b)–(d) by applying −135 V (Fig. 1(b)), removing the field (Fig. 1(b)), or by applying +135 V (Fig. 1(c)) and then removing the field (Fig. 1(d)). We note the twin arrangement formed when −135 V was applied, with {1 1 0} twin planes aligned perpendicular to the electric field, is stable to the removal of the electric field while the configuration formed in the same grains by reversing the electric field, where the twin planes predominantly lie at 45° to the field direction,

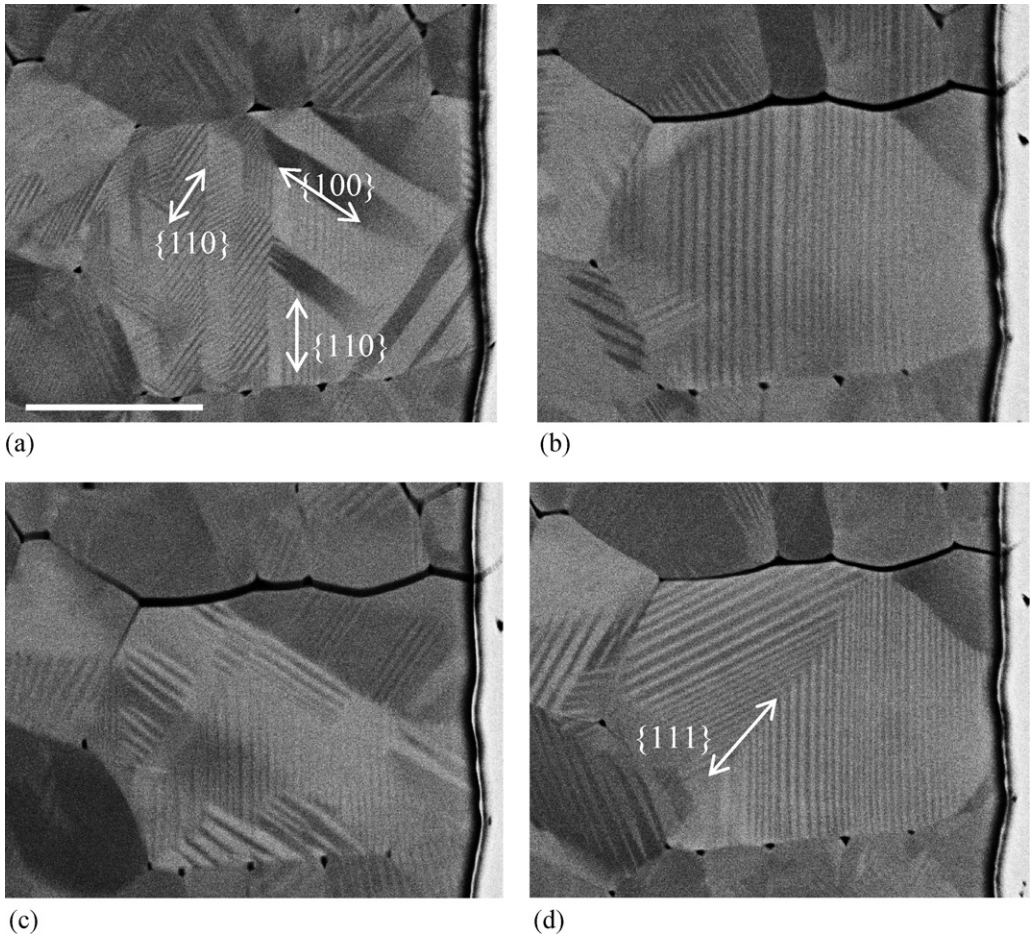

Fig. 1. BS imaging of a PZT grain subject to a static electric field. (Scale bar = 5 μm.) (a) Initial microstructure showing domain twinning, (b) microstructure when −135 V was applied between electrodes, (c) microstructure when +135 V was applied between electrodes, and (d) after removal of voltage.

becomes unstable when the electric field is removed and the associated strain changes. In these circumstances the twin planes realign, so that about 50% of the grain now has twin boundaries oriented at 90° to the field direction, indicating a preference for this 'orthogonal' twin configuration after domain switching by external electric fields.

In our experiments it was necessary to apply a minimum inter-electrode voltage of ±135 V in order to achieve large scale domain wall movement. For our electrode separation of 20 μm, this voltage gives a maximum electric field, at the sample surface, of 6.75 MV m^{-1}, while below the surface the field strength will reduce rapidly towards zero with depth. The surface value is significantly larger than the typical 2–3 MV m^{-1} usually quoted as necessary to achieve large scale domain wall movement in PZT and reflects the constraining effect of the bulk material, where the field is reduced, on the near-surface behaviour: until the field reaches a critical value throughout a significant volume of material this elastic constraint inhibits bulk domain wall movement.

3.3. Cyclic field behaviour

A second region of the ceramic was selected and subjected to cyclic strain by applying a 20 Hz sinusoidal alternating voltage via the surrounding pair of electrodes. The loading was delivered in pulses of 4-cycles and at progressively increasing voltages from ±20 V to ±160 V in 20 V steps. Each pulse terminated at the same point in the cycle (RH electrode positive) and the microstructure was observed after the field was removed. During these experiments the microstructure remained unchanged with no observable variation in the domain pattern and no surface cracking. Fig. 2(a) shows a BS image of the entire inter-electrode region after these pulses, with the electrode edges visible at the left and right hand sides of the image.

Following on immediately from this, the area was subjected to four further cycles with a peak voltage of ±180 V. This resulted in the nucleation and propagation of a crack, which followed an intergranular path from the left electrode towards the centre of the inter-electrode region (Fig. 2(b)). Domain wall movement, leading to a macroscopic realignment of the twin planes, can also be seen in several grains (arrowed): many major twin planes in these areas are now tending to orientate approximately perpendicular to the applied field direction.

Fig. 2(c) shows the microstructure after a further 20 cycles at ±180 V (i.e. a total of 24 cycles at this voltage). The first crack has continued to grow while a second crack has nucleated to the right of the region (arrowed), propagating along an inter-

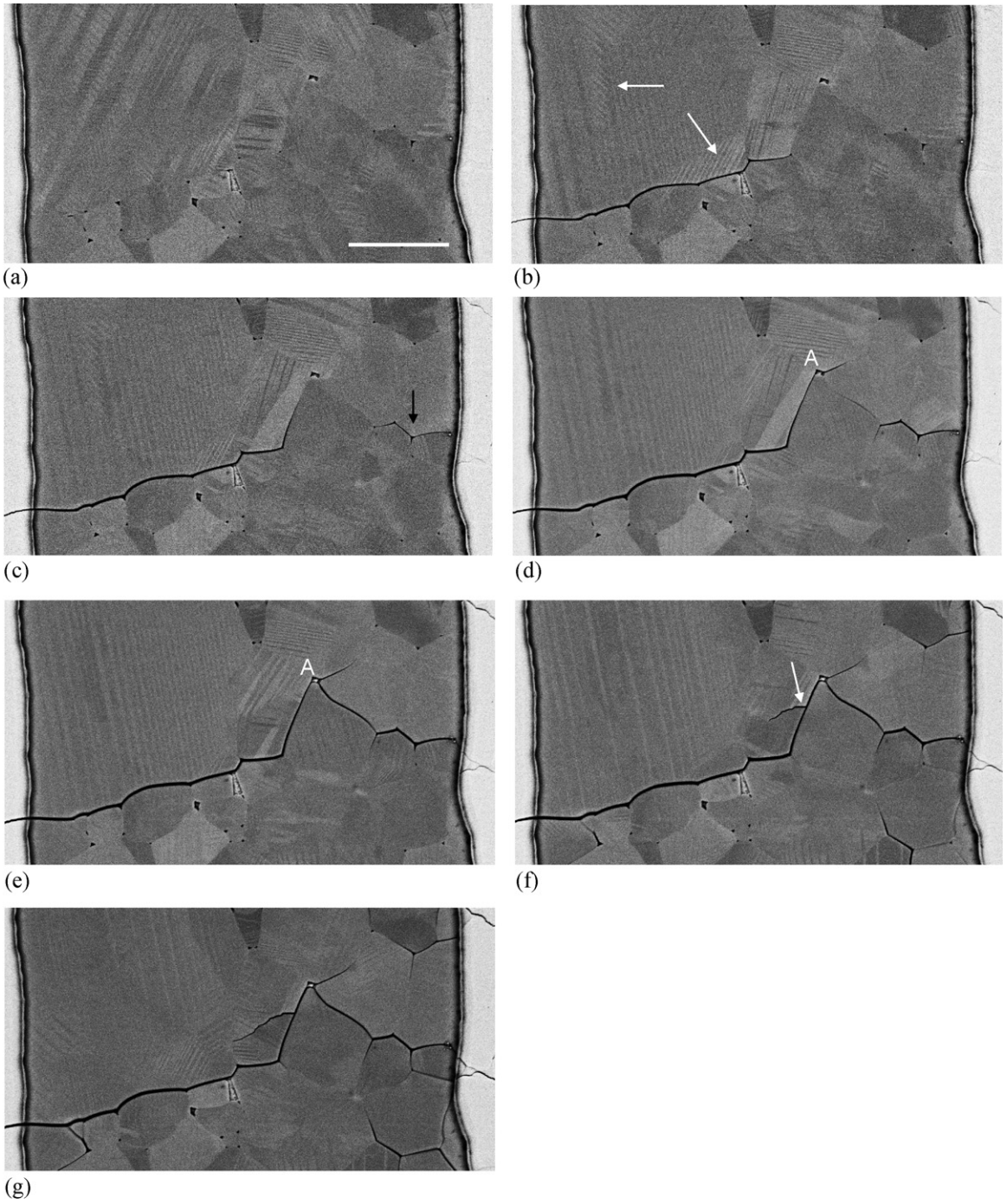

Fig. 2. BS imaging of area subjected to cyclic loading with an amplitude of ±180 V. (Scale bar = 5 μm.) (a) Initial microstructure, (b) after 4 cycles, (c) after 24 cycles, showing the nucleation of a second crack (arrowed), (d) after 60 cycles, showing crack interaction with a pore at 'A', (e) after 100 cycles, (f) after 1100 cycles, and (g) after 4100 cycles.

granular path parallel to the first crack, and following a series of triple junction pores. After 60 cycles the original crack has extended just beyond the pore at 'A' (Fig. 2(d)), and is continuing to propagate along a grain boundary in a direction nearly parallel to the electric field. After a total of 100 cycles the crack has propagated sufficiently for the curvature of this grain boundary to deflect it away from the field direction. As a result this crack stops growing and fracture continues instead along a second intergranular crack that has nucleated from pore 'A' along a similarly oriented, but presumably more energetically favoured, grain boundary, following a path that eventually joins the other crack (Fig. 2(e)).

After 1100 cycles the microstructure has evolved to that shown in Fig. 2(f). A transgranular crack (arrowed) has nucleated from the original intergranular crack on a grain boundary that is oriented at a high angle to the electric field direction. After a total of 4100 cycles (Fig. 2(g)), more intergranular cracks have developed, many with propagation

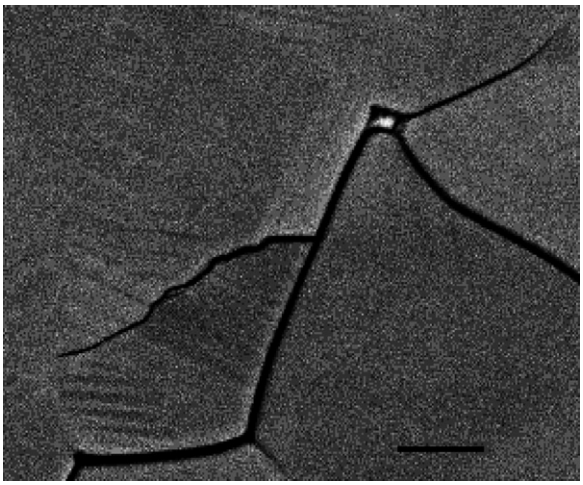

Fig. 3. BS image showing path of transgranular crack. (Scale bar = 1 μm.)

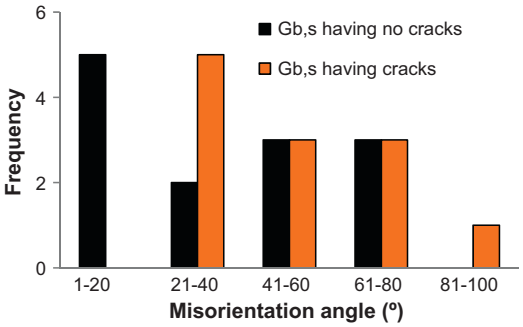

Fig. 4. Histograms showing misorientation of [1 0 0] vector across grain boundaries with and without cracking.

directions broadly aligned with the applied electric field. The transgranular crack has continued to grow parallel to the electric field direction. As was also observed for static loading, the preferred crack path in our sample, at least initially, is intergranular and generally parallel to the electric field.

Fig. 3 shows the transgranular crack in more detail, after 4100 cycles. The point on the grain boundary where it nucleated coincides with an abrupt change in the domain microstructure within the grain, defined by a {1 0 0} twin plane that separates two regions containing different twin alignments, so that during cyclic loading the domains on either side of the large {1 0 0} twin plane strain unevenly and distort the grain boundary plane [25]. A change of domain structure associated with the 90° reorientation, in particular, is known to lead to high stresses at the grain boundary [26], and the resulting stress concentration is relaxed by further cracking. The crack initially propagates through the grain along the {1 0 0} plane that separates the two regions, but as it continues its path is repeatedly deflected as it crosses domain boundaries, although it remains broadly aligned with the applied field direction. The deflection of the crack path by domain walls is believed to occur because crack propagation is driven by the stresses acting at the crack tip: the piezoelectric strains associated with the domain interfaces increase the elastic energy locally, favouring fracture along domain walls to relieve this stress [27].

Other studies of crack propagation in unconstrained PMN–PT [21] and PZT [22] ceramics subjected to cyclic loading have indicated that the preferred direction for crack growth is perpendicular to the applied electric field. However in a constrained (multilayer) sample of PMN crack propagation parallel to the applied field was observed [28]. In our experiments the electrode geometry means that there is a significant reduction in electric field strength, and hence mechanical strain, with depth below the sample surface. This strain gradient will impart a compressive force on surface cracks, and since, neglecting small local-microstructure controlled perturbations, the maximum distortion is aligned with the field direction, this effect will be most marked on cracks aligned perpendicular to the field direction, and crack propagation in this direction will be inhibited. The strain gradient will affect cracks aligned parallel to the field much less. Thus in our samples the constraining effect of the non-uniform field is believed to influence strongly the fracture behaviour and the favoured crack propagation direction.

Fig. 4 shows the distribution in misorientation of the [1 0 0] vector across grain boundaries within the area shown in Fig. 3(g), categorised according to whether the grain boundary is cracked or uncracked. Although the sample size is small, there is a clear indication that crack formation and propagation along grain boundaries with low misorientation angles is not favoured, with no cracks present for interfaces where the misorientation angle is less than 20°. Such low-angle grain boundaries are generally believed to be of lower energy than grain boundaries where there is a high misorientation [29]. Consequently on fracture they release less energy than high-angle grain boundaries, reducing the driving force for crack nucleation and propagation along these interfaces.

3.4. Displaced charge

A series of local hysteresis loops, showing displaced charge (Q) vs. applied voltage (V), was collected from the area shown in Fig. 3 at various stages during the ageing experiments. Fig. 5(a) shows the initial behaviour with increasing applied voltage, in 20 V steps from ±20 V up to ±160 V, corresponding to the cycling experiments described around Fig. 2(a). The data are presented as Q–V, rather than polarisation vs. electric field (P–E), due to the variation in electric field strength with depth that occurs within the sample as a consequence of the electrode geometry. As V is increased, the size of the loop and hence the hysteresis increases systematically, although the curves essentially maintain the same (lozenge) shape. The overall polarisation does not saturate for any of the loops in this voltage range, i.e. for this electrode geometry as V increases, so does the maximum displaced charge (Q_0) (Fig. 5(b)). This happens because the applied electric field, and hence also polarisation, decrease rapidly with depth below the surface of the sample. As the field is increased the affected region extends progressively deeper, meaning that part of the affected volume contributing to the overall response is always unsaturated. Nevertheless changes to these loops as a result of cycling can still provide

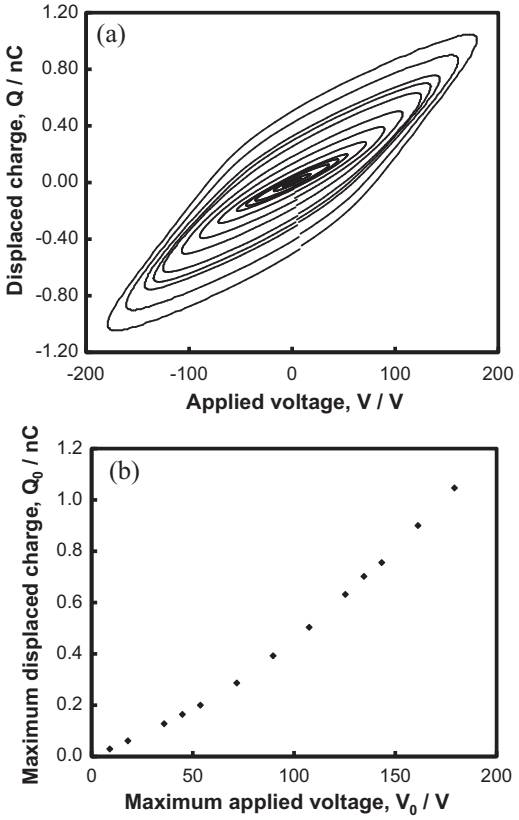

Fig. 5. (a) Hysteresis loops as a function of maximum applied voltage (V_0) in 20 V steps from 20 V to 160 V and (b) maximum displaced charge, Q_0, as a

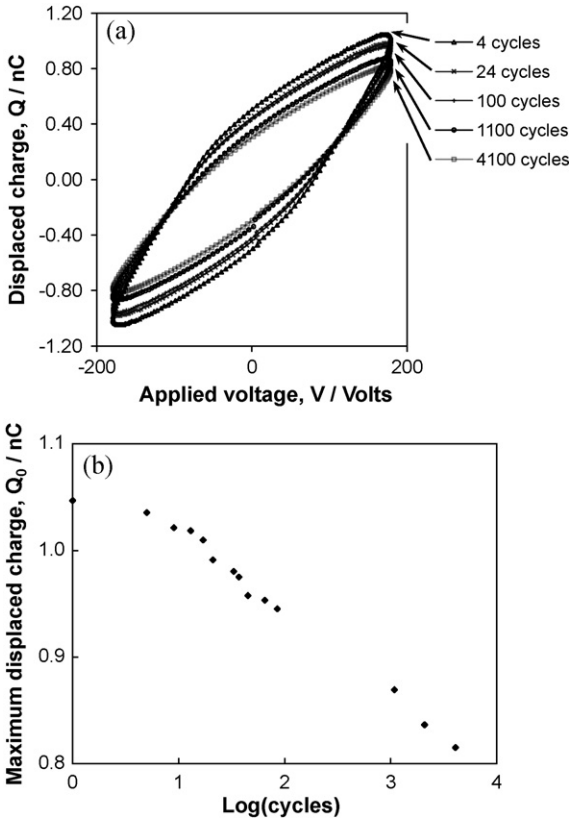

Fig. 6. Evolution of (a) hysteresis loops and (b) Q_0 with cycles during ageing at ±180 V.

a useful indication of electrical degradation within the material. Fig. 6(a) presents such a series of hysteresis loops, collected using a peak applied voltage of ±180 V after 4, 24, 100, 1100 and 4100 cycles, which correspond to the microstructural images shown in Fig. 2(b), (c), (e), (f) and (g) respectively. As the cycle count is increased the loops evolve due to decreases in the maximum polarisation, remnant polarisation, and coercive field. The net consequence of these changes is that with increasing cycles the hysteresis loop appears to rotate systematically clockwise. The decrease in Q_0 is linear with log(cycles), as shown in Fig. 6(b): such behaviour is consistent with cumulative fatigue damage due to the steadily increasing density of micro-cracks in the affected area.

4. Conclusions

Local domain switching and micro-cracking in PZT, caused by the application of static and cyclic electric fields was characterised by direct observation in the SEM. Twin planes were found to align preferentially perpendicular to the electric field direction when E_C was exceeded. Cracks were observed to nucleate at grain boundaries and propagate mainly along intergranular paths. When the grain boundary followed by the propagating crack becomes unfavourably oriented, so that the crack path deviates significantly from parallel to the electric field, propagation continued through the nucleation and growth of a new crack along a different grain boundary. In an extreme case a transgranular crack, aligned parallel to the field direction, nucleated at a position of high stress on an unfavourably oriented grain boundary. The preference for crack growth parallel to the electric field direction was explained in terms of compressive surface forces generated by the stress field developed within the sample when a voltage was applied. Hysteresis loops of the local area, showing the relation between applied voltage and displaced charge, did not show full saturation due to the reduction in electric field intensity with depth within the sample. During fatigue experiments a systematic decrease in maximum polarisation, remnant polarisation and E_C was observed, and was correlated with increasing microstructural damage.

References

[1] Y. Xu, Ferroelectric Materials and Their Applications, Elsevier, Amsterdam, 1990.
[2] M.E. Lines, A.M. Glass, Principles and Applications of Ferroelectrics and Related Materials, Oxford University Press, Oxford, 2001.
[3] X.F. Li, K.Y. Lee, Three-dimensional electroelastic analysis of a piezoelectric material with a penny-shaped dielectric crack, J. Appl. Mech.: Trans. ASME 71 (2004) 866–878.
[4] R.M. McMeeking, Crack tip energy release rate for a piezoelectric compact tension specimen, Eng. Fract. Mech. 64 (1999) 217–244.
[5] R.E. Newnham, Q.C. Xu, S. Kumar, L.E. Cross, Smart ceramics, Ferroelectrics 102 (1990) 77–89.
[6] S. Winzer, M. Shanker, A.P. Ritter, Designing co-tiered multilayered electrostrictive actuators for reliability, J. Am. Ceram. Soc. 72 (1989) 2246–2257.
[7] W. Yang, T. Zhu, Fracture and fatigue of ferroelectrics under electric and mechanical loading, Fatigue Fract. Eng. Mater. Struct. 21 (1998) 1361–1369.

[8] F. Fang, Y.H. Li, W. Yang, Effect of poling directions on the electric-field-induced fatigue crack growth in $BaTiO_3$ single crystals, Ferroelectrics 322 (2005) 11–21.
[9] Z. Chen, Z. Lu, X. Chen, Y. Zhang, X. Cheng, Effects of electrical characters on electrical fatigue behaviour in PLZT ferroelectric ceramics, in: Proc.: High Performance Ceramics III, Key Eng. Mater. 280–283 (2005) 159–162.
[10] W. Li, A.P. Chen, X.M. Lu, J.S. Zhu, Y.N. Wang, Priority of domain wall pinning during the fatigue period in bismuth titanate ferroelectric thin films, Appl. Phys. 86 (2005) 1–3 (Letters).
[11] J.S. Liu, S.R. Zhang, L.S. Dai, Domain evolution in ferroelectric thin films during fatigue process, J. Appl. Phys. 97 (2005), 104102-1–104102-4.
[12] V.V. Shvartsman, A.L. Kholkin, C. Verdier, Z. Yong, D.C. Lupascu, Investigation of fatigue mechanism in ferroelectric ceramic via piezo-response force microscopy, J. Eur. Ceram. Soc. 25 (2005) 2559–2561.
[13] S.M. Yoon, N.Y. Lee, S.O. Ryu, W.C. Shin, I.K. You, B.G. Yu, Effect of ferroelectric switching time on fatigue behaviours of (1 1 0)- and (0 0 1)-oriented $(Bi, La)_4Ti_3O_{12}$ thin films, Thin Solid Films 484 (2005) 374–378.
[14] Q. Jiang, W. Cao, L.E. Cross, Electric fatigue in lead zirconate titanate ceramics, J. Am. Ceram. Soc. 77 (1994) 211–215.
[15] H. Cao, A.G. Evans, Electric-field-induced fatigue crack growth in piezoelectric, J. Am. Ceram. Soc. 77 (1994) 1783–1786.
[16] C.S. Lynch, W. Yang, L. Collier, Z. Suo, R.M. McMeeking, Electric field induced cracking in ferroelectric ceramics, Ferroelectrics 166 (1995) 11–30.
[17] T. Zhu, F. Fang, W. Yang, Fatigue crack growth in ferroelectric ceramics below the coercive field, J. Mater. Sci. 18 (1999) 1025–1027 (Letters).
[18] B. Liu, D. Fang, K.-C. Hwang, Electric-field-induced fatigue crack growth in ferroelectric ceramics, Mater. Lett. 54 (2002) 442–446.
[19] F. Fang, W. Yang, F.C. Zhang, H.S. Luo, In-situ observation of electrically induced fatigue crack growth for ferroelectric single crystals, in: IUTAM Symposium: Mechanics and Reliability of Actuating Materials, 2006, 32–39.
[20] Z. Xu, X. Tan, P. Han, J.K. Shang, In situ transmission electron microscopy study of electric-field-induced microcracking in single crystal $Pb(Mg_{1/3},Nb_{2/3})O_3$–$PbTiO_3$, Appl. Phys. 76 (2000) 3732–3734 (Letters).
[21] H. Wang, R.N. Singh, EF induced effect on the crack propagation in an PMN–PT ceramics, Ferroelectrics 168 (1995) 281–291.
[22] I. Westram, D. Lupascu, J. Rodel, Electric-field-induced crack initiation from a notch in a ferroelectric ceramic, J. Am. Ceram. Soc. 90 (2007) 2849–2854.
[23] Z. Xu, In situ study of electric field induced microcracking in piezoelectric single crystals, Mater. Sci. Eng. B 99 (2003) 106–111.
[24] M.I. Mendelson, Average grain size in polycrystalline ceramics, J. Am. Ceram. Soc. 52 (1969) 443–446.
[25] X. Tan, Z. Xu, J.K. Shang, In situ transmission electron microscopy observations of electric-field-induced domain switching and microcracking in ferroelectric ceramics, Mater. Sci. Eng. A 314 (2001) 157–161.
[26] Y. Zhang, Q. Jiang, Twinning induced stress and electric field concentrations in ferroelectric ceramics, J. Am. Ceram. Soc. 78 (1995) 3290–3296.
[27] X. Tan, H. Hui, In situ transmission electron microscopy studies of electric-field induced phenomena in ferroelectrics, J. Mater. Res. 20 (2005) 1641–1653.
[28] A.S. Raynes, G.S. White, S.W. Freiman, B.S. Rawal, Electric field effects on crack growth in a PMN ceramic, Ceram. Trans. 15 (1989) 129–142.
[29] D.R. Clarke, Intergranular phases in polycrystalline ceramics, in: Dufour, Monty, Petot-Ervas (Eds.), Surfaces and Interfaces of Ceramic Materials, NATO ASI Series V173, Kluwer, 1989, pp. 57–80.